Regular Article

INORGANIC CHEMISTRY RESEARCH
Published by the
Iranian Chemical Society
www.inorgchemres.org
info@inorgchemres.org

Inorg. Chem. Res., *Vol. 4, No. 1,103-122, July 2020*
DOI: 10.22036/icr.2020.233634.1068

Removal of Bisphenol-A by NaP Zeolite/Hydroxyapatite Composite: Adsorption Experiments and Modeling by Artificial Neural Networks

B. Shoshtari-Yeganeh[c], M. Zendehdel[a,b,*] and S.A.M. Leghaei[d]

[a]*Department of Chemistry, Faculty of Science, Arak University, Arak 38156-8- 8349, Iran*
[b]*Institute of Nanosciences & Nanotechnology, Arak University, Arak, Iran*
[c]*Environment Research Center, Research Institute for Primordial Prevention of Non-communicable Disease, Isfahan University of Medical Sciences, Isfahan, Iran*
[d]*Department of Electrical Engineering, Islamic Azad University Mobarakeh Branch, Isfahan, Iran*
(Received 1 June 2020, Accepted 23 July 2020)

In this paper, we have reported removal of Bisphenol A (BPA) by Hydroxyapatite/NaP zeolite (HAp:Zeolite) nanocomposite which synthesized in previous our work and characterized by using different methods such as X-ray diffraction, Fourier transform infrared spectroscopy, scanning electron microscope, Energy Dispersive X-ray analysis, surface area, and thermogravimetric analysis. To investigate the purification performance for removal BPA batch experiments were used. The results showed that the removal capacity could reach an equilibrium value of 11.125 mg g^{-1} in the initial BPA concentration of 50 mg L^{-1}. Some parameters such as initial concentration, pH, contact time, adsorbent dosage, and the temperature were studied that result shows this nanocomposite have high capacity for adsorption of BPA. The kinetic study presented that it agreed well with the pseudo-second-order model (R^2 = 0.994). Furthermore, thermodynamics studies were carried out, and result showed an exothermic condition for adsorption process. An artificial neural networks (ANNs) model was developed to predict the performance removal process based on experimental information which shows an association between the predicted results of the designed ANN model and experimental data. Results showed that the neural network model predicted values are found in close agreement with the batch experiment result with a correlation coefficient (R^2) about 0.99051 and mean squared error 0.005938.

Keywords: Batch mode, Bisphenol A, Hydroxyapatite/Zeolite nanocomposite, Artificial neural networks

INTRODUCTION

The increasing population and urbanization of society caused to develop some products which distribution of toxic chemicals, containing the endocrine-disrupting chemicals (EDCs) in the environment [1]. Many EDCs excluding natural estrogens (*e.g.*, estrone (E1), 17b-estradiol (E2), and estriol (E3)), synthesized estrogen (*e.g.* ethinylestradiol (EE2)), and industrial compounds (*e.g.*, bisphenol A (BPA CAS Registry No. 80-05-7) and nonylphenol) are organic compounds that have various adverse health effect in the recent years [2]. Structures and physicochemical properties of EDCs cause to occupy the binding acceptor sites of the hormone receptors, so endocrine systems may be disrupted that this is an environmental risk for animals and humans [3,4]. One of the known endocrine disruptors is Bisphenol A (BPA; (2,2-bis(4-hydroxyphenyl) propane)) contain two phenol rings connected by a methyl bridge (Fig. 1) that has important toxicity to aquatic organisms in the range of 1-10 mg mL^{-1} for freshwater and marine species [5,6]. BPA is widely used as a raw material for polycarbonate plastics, polyester, phenol resins, polyacrylates, epoxy resins, and lacquer coatings on food cans [7]. BPA can be leached from plastic containers into foods and drinks when they become

*Corresponding author. E-mail: m-zendehdel@araku.ac.ir

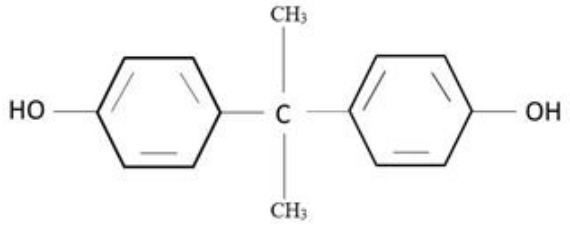

Fig. 1. Chemical structure of BPA.

heated or broken [8]. Also, BPA have various adverse effects, such as increasing breast and prostate cancer, obesity, and insulin-resistant [9]. Unfortunately, by increasing usage of products with base of BPA, the probability of environmental pollution by BPA has been developed. Literature review show that BPA has been detected in all types of l waters at variable concentrations such as hazardous waste landfill leachate up to 17.2 mg L^{-1} [10], 12 mg L^{-1} stream water [11], and 0.1 mg L^{-1} in drinking water [12]. The production and application of BPA are rising with the increasing plastics, and the global production of BPA was 3.9 million tons in 2006 and increased to 4.7 million tons in 2008 [13]. Due to the widespread utilization of BPA, there is increasing interest in effective remediation technologies for its removal from contaminated water. Some methods such as, adsorption [14], membrane separation [15], solvent extraction [16] and photodegradation [17] are used. Among these methods, adsorption is widely used to remove refractory trace compounds with a high potential of adsorption because of simplicity and high efficiency.

Literature reviews show that porous materials such as zeolite have a good potential for adsorption of small gas, liquid molecule, and Hazard materials [19] and also Hydroxyapatite (HAp, $Ca_{10}(PO_4)_6(OH)_2$) that is the main mineral essential of vertebrate skeletal systems and used as an adsorbent in the purification of wastewater [20]. In our previous work, HAp:NaP zeolite nanocomposite shows good effectiveness in the removal of some cationic and anionic hazard materials. The advantage of this nanocomposite can be attributed to their high specific area, large pore volume, chemical inertness, low cost, and good mechanical stability [21].

Recently artificial neural networks and their application in control strategies have been widely used to achieve a good yield. The use of neural networks to model uncertain nonlinear functions within the geometric control technique has been demonstrated by several researchers [22]. Artificial Neural Network (ANN) is categorized as an artificial intelligence modeling technique due to their ability to recognize patterns and relationships in historical data and subsequently make inferences concerning new data. ANNs can be used for two broad categories of problems: data classification and parameter prediction [23]. The main applications of the ANN technique in the water treatment industry are in the development of process models and model-based process control and automation tools [24]. ANN models of the drinking water treatment process can assume two distinct forms: (i) process models and (ii) inverse process models. (i) The process model predicts the value of one or more process outputs if given the values of the process input parameters. An example of this type of model is the prediction of clarifier effluent turbidity using influent water parameters and operational parameters. (ii) The inverse process model predicts the value of one or more process inputs if given the values of the remaining process inputs and process output(s). This type of model is often used to predict the value of an operational parameter required to reach a target effluent quality [25].

The objective of the present study is the investigation of the feasibility for the removal BPA from water at ambient temperature by HAp:NaP zeolite nanocomposite. Also, we achieved optimum conditions such as pH, adsorbent dosage, initial concentration, and temperature as variable parameters.

Also in this work, an artificial neural networks (ANNs) model type (i) was developed to predict the performance adsorption process over synthesized adsorbent based on data from bath experiments which was considered for the first time. A comparison between the predicted results of the designed ANN model and experimental data was also conducted. The result shows that the HAp:NaP nanocomposite is an effective adsorbent for the removal of BPA from an aqueous solution that is remarkably high compared with the reported materials.

EXPERIMENTAL

Materials and Instruments

Different chemicals materials that used in the current study were of analytical grade. Calcium nitrate (CNT), potassium dihydrogen phosphate (KPP), ammonia, and deionized water were used for the preparation of Hydroxyapatite and also silica gel, sodium hydroxide, and aluminum hydroxide were used for the preparation of zeolite. Nitric acid (0.1 N) and sodium hydroxide (0.1 N) was used for adsorption/desorption study (Merck Company supplied all chemical materials), and BPA (≥ 99) was purchased from Sigma Company.

An X-ray powder diffraction (XRD) was analyzed by a Philips X'Pert diffractometer operating with Cu-Kα radiation, FT-IR of the samples was characterized by Unicom Galaxy Series FT-IR 5000 in the region of 200-4000 cm^{-1}, SEM micrograph images were acquired by a Philips XL30 electron microscope, The specific surface areas and pore volume of the adsorbent were estimated by nitrogen adsorption at relative pressures (P/P0) in the range of 0.008-0.5 that recorded by Belsorp mini II, The thermal analysis TG/DTA curves were measured by a Diamond TG/DTA Perkin Elmer thermo analyzer and the final concentration of BPA was measured by HPLC-Waters 515 that equipped by UV-Vis detector.

Sample Preparation and Characterization Methods

In the first step, zeolite gel with the molar composition $16Na_2O:Al_2O_3:15SiO_2:320H_2O$ was prepared and aged for five days. For the preparation of HAp:Zeolite nanocomposite, different amounts of HAp (0.12, 0.24, 0.36, 0.48 g) were added to zeolite gel, and this mixture was stirred for 15 min continuously. In order to prepare nanocomposite, the mixture was then placed in an autoclave at 100 °C for 26 h. the precipitated sample filtrated and washed with deionized water repeatedly until to reach a pH of 7. The resulting product was dried at room temperature for 24 h and characterized [21].

Experimental Procedures

At first, 1000 mg L^{-1} stock solution of bisphenol A (BPA) was prepared by dissolve 0.5 g in 500 mL of methanol. The BPA solutions desired solution was obtained by serial dilution of 1000 mg L^{-1} BPA solution. The bisphenol A adsorption experiments from its aqueous solution by HAp:Zeolite nanocomposite with different content of HAp were carried out using 20 mg L^{-1} solution. 4 g L^{-1} of adsorbent was added to 25 mL of BPA solution in ambient temperature and pH of 7. After continuous stirring for 60 min, adsorbent filtrated. BPA concentration was recorded by high-performance liquid chromatography (HPLC) system. The UV detector was set at a wavelength of 275 nm. Effect of initial concentration (5, 10, 15, 20, 25, 30, 40, 50 mg L^{-1}), pH (5, 6, 7, 8, 9, 10, 11, 12), adsorbent dosage (1, 2, 3, 4 mg L^{-1}), contact time (15, 30, 60, 90, 120 min) and temperature (25, 35, 45 °C) was examined. Equilibrium diagram of BPA was drawn in a range of 1-40 mg L^{-1}, and its equation were used to calculate the concentration of BPA (Fig. 2).

Amount of BPA adsorbed, q_e (mg g^{-1}) was determined using the equation:

$$q_e = \frac{(C_0 - C_e)V}{W} \quad (1)$$

Where C_0 is the initial BPA concentration (mg L^{-1}) and C_e is the equilibrium concentration (mg L^{-1}), respectively. q_e (mg g^{-1}) is the amount of adsorbate adsorbed per unit mass of adsorbent, V, the volume of BPA solution (in liter) and, W is the weight of HAp:Zeolite nanocomposite (in grams).

The removal efficiency of BPA (%) from aqueous solution by HAp:Zeolite nanocomposite was calculated using the following equation:

$$\%\,\mathrm{Re}moval = \frac{C_0 - C_e}{C_0} \times 100 \quad (2)$$

RESULTS AND DISCUSSION

Characterization of HAp:Zeolite nanocomposite

Pure zeolite, hydroxyapatite, and Hydroxyapatite: Zeolite nanocomposite with a variety amounts of HAp (1:1, 2:1, 4:1, 6:1) was characterized by X-ray diffraction and FT-IR spectrometer that reported in our previous work [26]. Furthermore, Tables 1 and 2 showing the main peaks recorded by X-ray diffraction and FT-IR spectrometer,

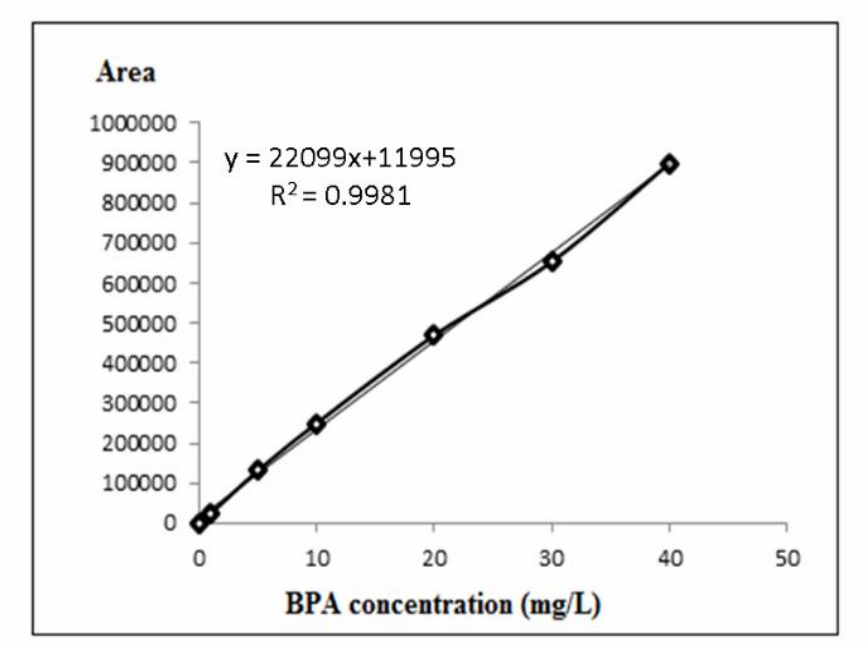

Fig. 2. Equilibrium diagram of BPA.

Table 1. Main Data of X-Ray Diffraction

Sample	2Theta
NaP zeolite	12.46 17.66 21.67 28.10 33.38
Hydroxyapatite	25.96 29.01 31.831 32.88 34.1757 39.97 46.87
Hydroxyapatite:Zeolite (1:1)	12.63 17.91 21.83 26.03 28.31 29.59 31.97 32.41 33.65
Hydroxyapatite:Zeolite (2:1)	12.31 17.99 21.77 25.87 28.87 29.49 31.13 32.67 33.01
Hydroxyapatite:Zeolite (4:1)	12.46 17.16 21.86 25.91 28.98 29.46 31.82 32.18 33 34.20 39.84 46.74
Hydroxyapatite:Zeolite (6:1)	12.54 17.66 21.7 25.88 28.02 29.34 31.86 32.02 33.34 39.32 46.86

respectively.

The XRD pattern for all samples show a peak about 2θ = 29° which confirm the presence of Hydroxyapatite in the nanocomposite with a different ratio. The low intensity of this peak can be due to the incorporation of HAp to channel of zeolite or size of Hydroxyapatite (~ 8 nm) that in agreement with other reported [27-29]. Table 2 show the main bands of Hydroxyapatite, Zeolite, in the FT-IR of Hydroxyapatite:Zeolite nanocomposite with different ratios of HAp. The bands at 437 cm^{-1} and 799 cm^{-1} are assigned to

Table 2. Main Data of FT-IR Spectrometer

Sample	Bands (cm^{-1})
Zeolite NaP	437 605 799 1012 1653 3466
Hydroxyapatite	435 609 854 962 1035 1456 1660 3572
Hydroxyapatite:Zeolite (1:1)	435 605 742 1028 1458 1653 3533
Hydroxyapatite:Zeolite (2:1)	437 607 746 1006 1487 1654 3466
Hydroxyapatite:Zeolite (4:1)	437 608 756 1019 1469 1652 3502
Hydroxyapatite:Zeolite (6:1)	436 609 788 968 1033 1491 1656 3566

TO_4 (T = Si, Al) bending mode and amorphous SiO_2 stretching vibration respectively and the band at 1012 cm^{-1} corresponded to internal tetrahedral asymmetrical stretching [30]. The two bands at 3466 and 1653 cm^{-1} are corresponding to the hydroxyl group stretching vibration and H-O-H bending vibration, respectively [31]. Stretching vibration of OH for the hydroxyapatite lattice was showed by the band at 3574 cm^{-1} and two bands at 1456 cm^{-1}, and 854 cm^{-1} are attributed to carbonate group [32] and also, the band at 1035 cm^{-1} and the band at 962 cm^{-1} are assigned to P=O stretching vibration of PO_4^{3-} and symmetric P=O stretching vibration (ν1). Moreover, the band at 474, 567 and 601 cm^{-1} have corresponded to the ν2 and ν4 bending vibration of the phosphate group [32].

Based on the the results for nanocomposite with different ratio of HAp, the characteristic band of Hydroxyapatite and zeolite are shown in them, This result reveals both hydroxyapatite and NaP phases present in the composite.

The SEM micrograph images for HAp: Zeolite nanocomposite with different ratios (1:1, 4:1, 6:1) that have high activity for BPA removal was shown in Figs. 3a-d. Similar to other observation found in the literature, both cactus-like and diamond-like morphology with the 1-2 μm size of each were appeared in the SEM image [33]. Also, with increasing the percentage of HAp, diamond-like morphology for NaP zeolite can be observed.

The BET data for the HAp: Zeolite ratio 1:1 and 4:1 are 35.62 $m^2\ g^{-1}$ and 30.23 $m^2\ g^{-1}$, respectively, which are smaller than of NaP zeolite (45 $m^2\ g^{-1}$) which confirm the introducing of nano Hydroxyapatite to zeolite channels [21]. Figure 4 shows the TG/DTA for HAp:Zeolite nanocomposite with a ratio of 1:1. The TG curve exhibits three mass loss steps, in the first step in the temperature range 30-200 °C is attributed to losses of adsorbed water (12.85%) in Hydroxyapatite and Zeolite. The second steps, in the temperature range of 200-500 °C (5.06%) is demonstrated to condensation of hydrogen phosphate groups to form pyrophosphates ($P_2O_7^{2-}$) in the Hydroxyapatite and also removal of the hydroxyl groups in the zeolite. The third steps in the temperature about 800 °C (4.43%) is related to the phase transformation of zeolite and the conversion of $P_2O_4^{4-}$ to PO_4^{3-} form [34,35].

Adsorption Procedure

Effect of adsorbent type. At first, four types of HAp:Zeolite with different content of HAp were used as an adsorbent for the removal of BPA from aqueous solution. All parameters include contact time, temperature, pH, initial concentration of BPA, and adsorbent dosage keeping constant. As shown in Table 3, HAp:Zeolite, with a ratio of 1:1 was showed the highest effect respect to other adsorbents. So this adsorbent was used for further study.

Effect of pH value. Deprotonating of BPA has occurred in two pH. At first, it started at pH around pH 8 with $pKa_1 = 9.59$ and another one started at around pH 9 with

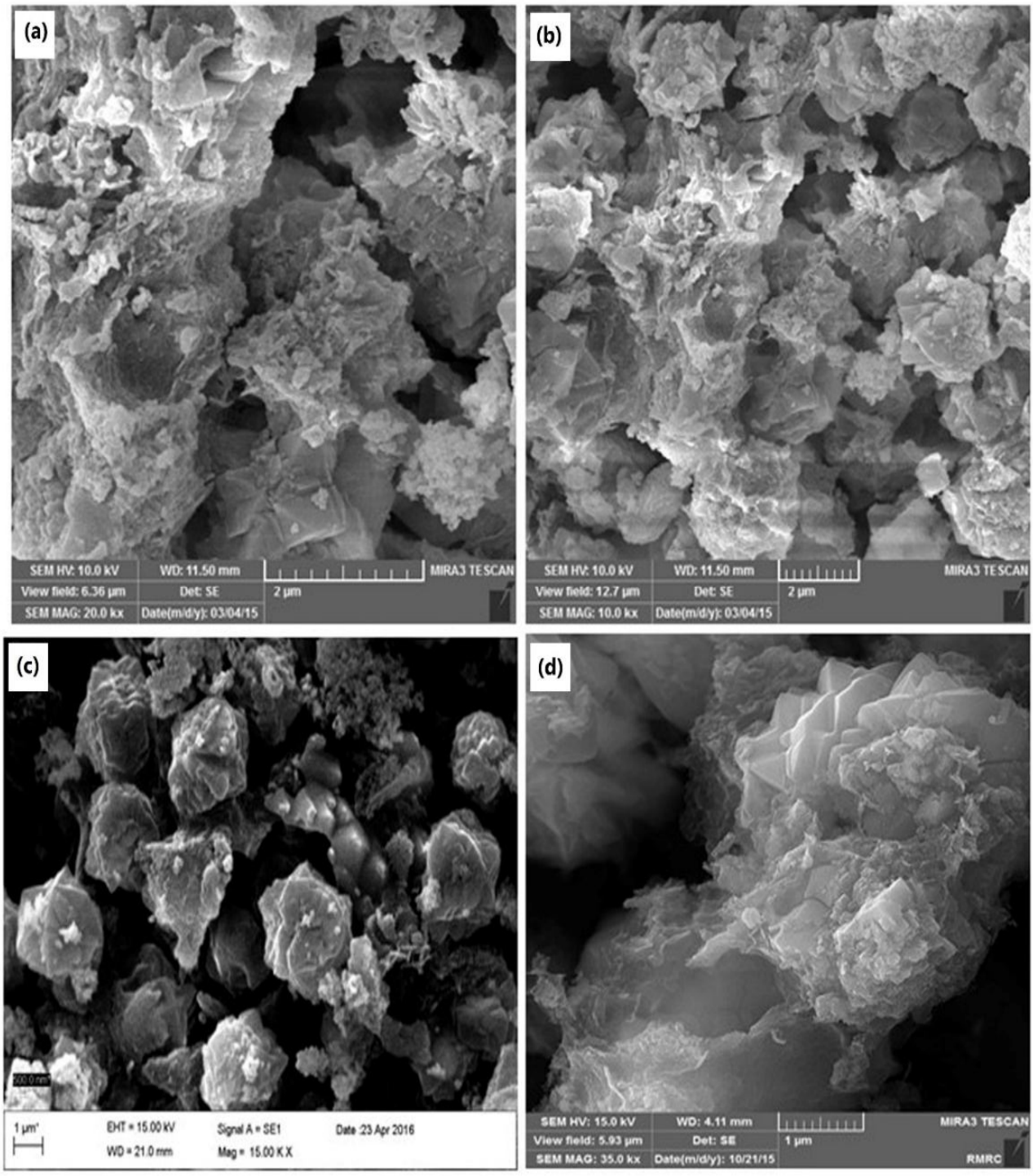

Fig. 3. SEM micrograph of Hydroxyapatite:Zeolite nanocomposite: (a,b) 1:1 ratio, (c) 4:1 ratio, (d) 6:1 ratio.

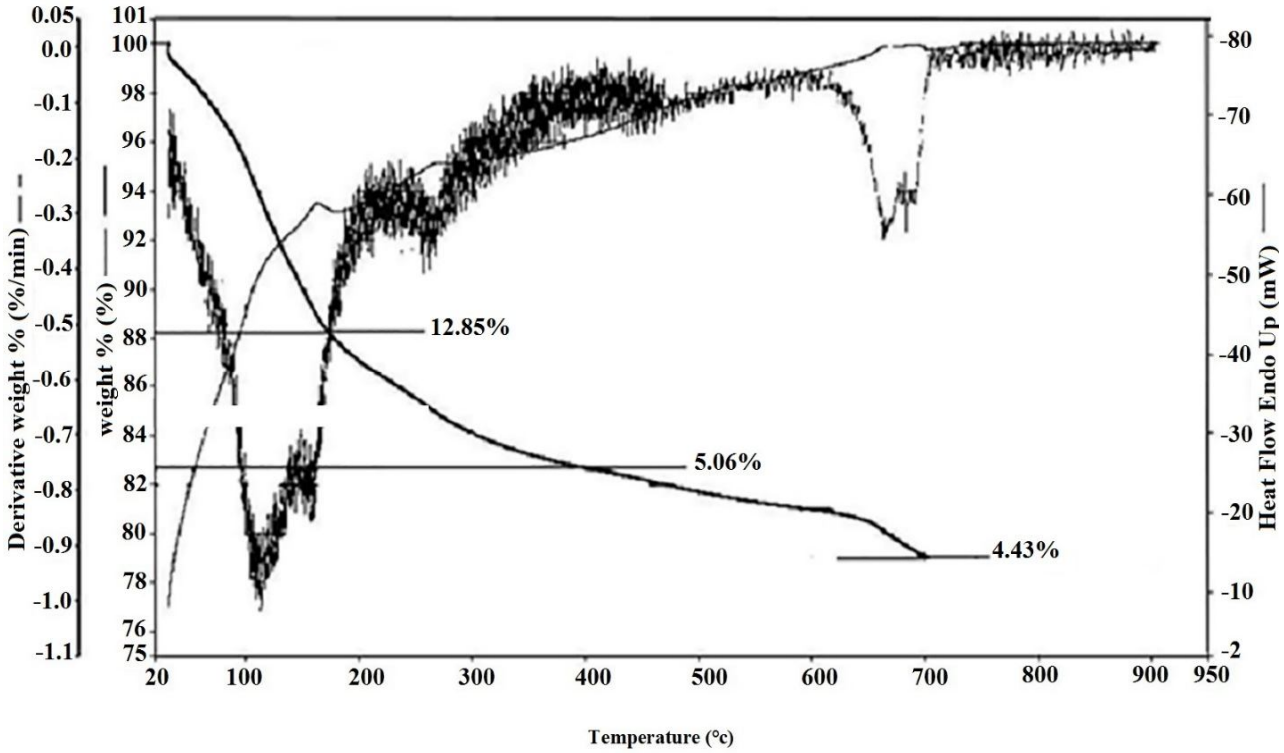

Fig. 4. TG/DTA curve of Hydroxyapatite:Zeolite with ratio of 1:1.

Table 3. EDX Data for Hydroxyapatite:Zeolite Nanocomposite

Sample	Ca	P	O	Ca/P	Na	Al	Si
Hydroxyapatite:Zeolite (1:1)	8.56	5.57	55.30	1.53	4.45	6.78	13.04
Hydroxyapatite:Zeolite (4:1)	13.55	8.39	53.74	1.61	4.43	6.38	14.68
Hydroxyapatite:Zeolite (6:1)	15.84	9.96	50.8	1.59	2.14	5.28	14.96

pKa_2 = 11.30 that were shown by following equations [36,37]:

$$H_2BPA \longrightarrow H^+ + HBPA^- \quad (1)$$

$$HBPA^- \longrightarrow H^+ + BPA^{2-} \quad (2)$$

Six different pH tests were carried out, and the results are shown in Fig. 5. Results indicated that adsorption capacity was decreased with increasing pH ranging from 5-12. However, in the range of 5-7, no significant change observed, indicating that there aren't significant binding affinity between the BPA molecule and nanocomposite under weak acidity and neutral condition. The occurrences can be due to the first and second deprotonation equilibrium of BPA, which happened at pH values above eight and more than half of BPA molecules were ionized into anion. Simultaneously, the surface charge of HAp:Zeolite due to the presence of HAp nanoparticles on the surface of zeolite is neutral at a pH of 6.7 (pHpzc) [38].

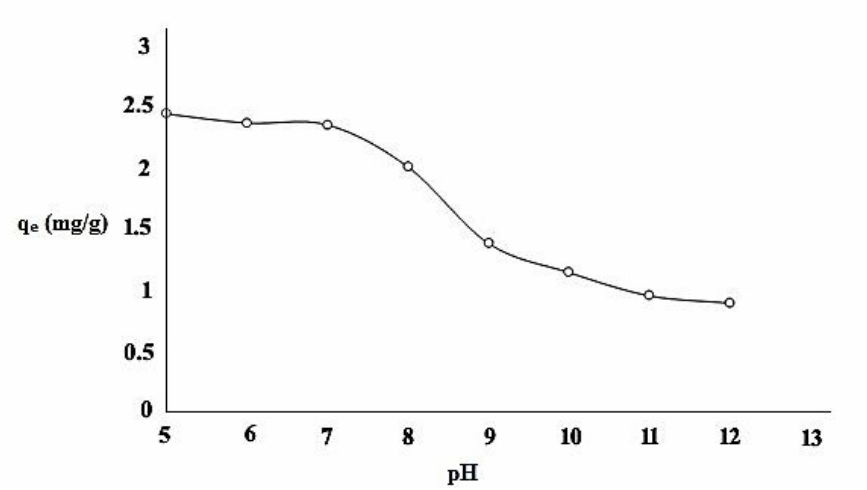

Fig. 5. Effect of pH on removal of BPA by HAP:Zeolite nanocomposite.

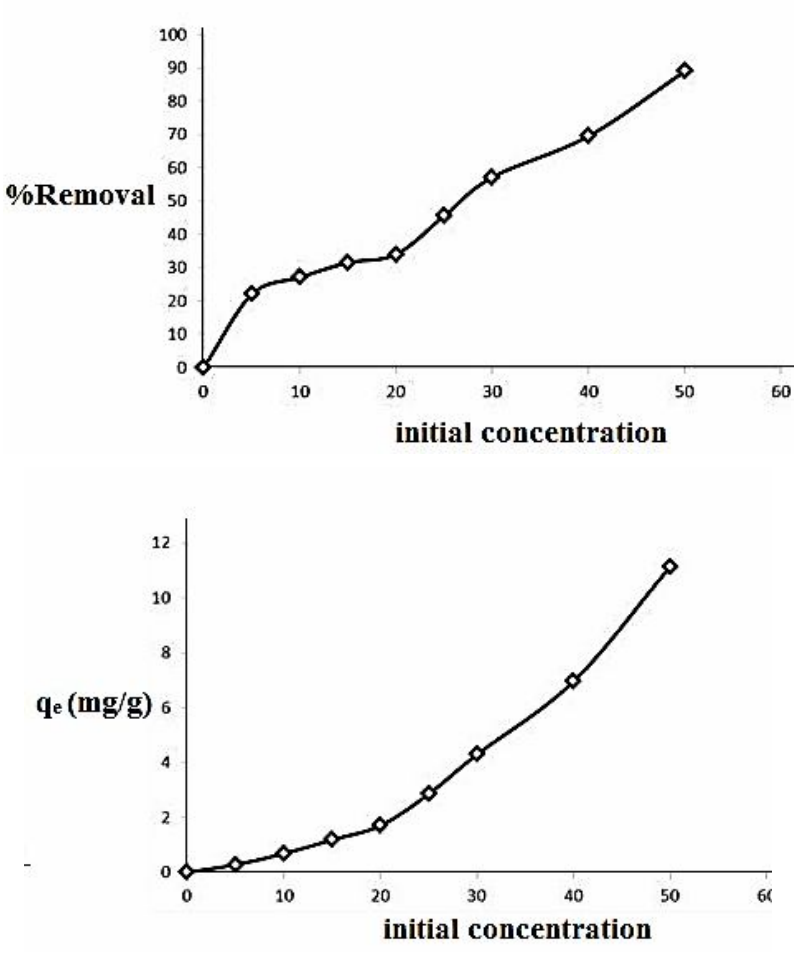

Fig. 6. Effect of initial concentration on removal of BPA by HAp:Zeolite nanocomposite.

Characterization of HAp:Zeolite nanocomposite by XRD and FT-IR was shown that HAp nanoparticles presented in the channel and surface of NaP zeolite so charge surface of HAp can be affected on the process of adsorption. Various reactions of hydroxyl groups and unequal adsorption from the solution of ions of opposite charge can be determined of charge on the surface of Hydroxyapatite [39,40].

Hydroxyapatite as salt has two types of groups that these are hydroxyl and phosphatic groups. The phosphatic groups have more acid character respect to hydroxyl. The reactions of surface groups at the Hydroxyapatite that make surface charge show as following [38]:

$$CaOH + H^+ \longleftrightarrow CaOH_2^+ \quad (3)$$

$$CaOH \longleftrightarrow CaO^- + H^+ \quad (4)$$

$$PO_4H \longleftrightarrow PO_4^- + H^+ \quad (5)$$

$$PO_4^- + Ca^+ \longleftrightarrow PO_4 + Ca^{2+} \quad (6)$$

Due to the nanocomposite's surface charge, when the solution pH is basic, the electrostatic repulsion occurred between BPA anion and negatively charged nanocomposite. Because of no significant changes in the range of 5-7, then, pH = 7 was selected as optimum pH for further study.

Effect of initial concentration. The effect of the initial concentration of BPA on the adsorption reaction was investigated by using BPA solutions in the range of 5-50 mg L^{-1}. All other parameters were kept constant (Fig. 6). The percentage removal of BPA by HAp:Zeolite nanocomposite increased from 22% to 89% by increasing initial concentration. The equilibrium adsorption capacity (q_e) increased as the initial concentration of BPA increased from 5 to 50 mg L^{-1}, revealing that a powerful driving force to overcome the mass transfer resistance between the aqueous and solid phases was provided by initial concentration [41].

Effect of contact time. Figure 7 shows the effect of contact time on the removal of BPA by HAp:Zeolite nanocomposite at 25 °C. The residual concentration of BPA in aqueous solution was measured at different contact times with an initial concentration of 50 mg L^{-1} and the nanocomposite dosage of 4 g L^{-1}. Results showed that rapid removal of BPA increased by increasing time from 15 until 60 min and then slows down until the equilibrium occurred at 120 min.

Pseudo-second-order kinetics was applied to investigate BPA adsorption characteristics (Fig. 8). Pseudo-second-order kinetics, the hypothesis of which states that the adsorption rate is controlled by chemical adsorption could be expressed in general as follow [42]:

$$(\frac{t}{q_t}) = \frac{1}{k_2\, q_e^2} + \frac{1}{q_e}(t) \quad (3)$$

Where k_2 is the rate constant of second-order rate adsorption in (g mg^{-1} min^{-1}), q_t is the amount of BPA absorbed by an adsorbent at any time (mg g^{-1}), q_e is equilibrium adsorption and can be calculated from the slope of the plot obtained by plotting versus t. furthermore, k_2 can be determined from the intercept of this plot. According to the high regression coefficient (R^2 = 0.994), the kinetic of BPA adsorption onto HAp:Zeolite nanocomposite fits well with the pseudo-second-order kinetic model. Good accordance with experiment data with the pseudo-second-order model revealed that the removal process might be a chemical process between adsorbent and BPA.

Effect of adsorbent dosage. The effect of different dosages of HAp:Zeolite nanocomposite on Bisphenol-A with an initial concentration of 50 mg L^{-1}, pH of 7, 60 min agitation time at 25 °C has been carried out. As shown in Fig. 9, the percent removal of BPA was increased from 56.2% to 83.8% by increasing adsorbent dosage from 1 to 4 g L^{-1}. This pattern is undoubtedly due to the increase in the available surface area per gram of sorbent.

Effect of temperature. Temperature is an important parameter in the influencing the adsorption process. Thermodynamic parameters include, enthalpy change (ΔH°), entropy change (ΔS°) and free energy change (ΔG°) were applied to investigate adsorption process in three different temperatures (25, 35, 45 °C). The changes in these parameters of adsorption can be determined by the following equations [43]:

$$\log K_c = \frac{\Delta S}{2}.303R - \frac{\Delta H}{2}.303RT \quad (4)$$

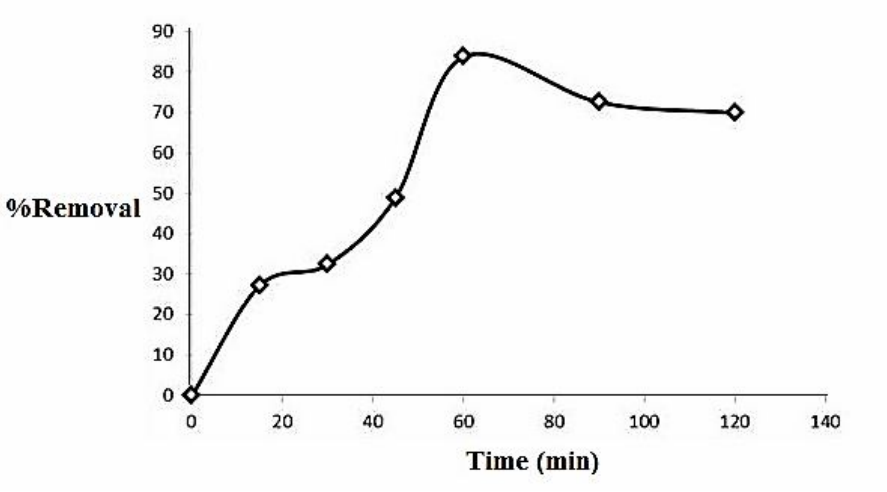

Fig. 7. Effect of contact time on removal of BPA by HAp:Zeolite nanocomposite.

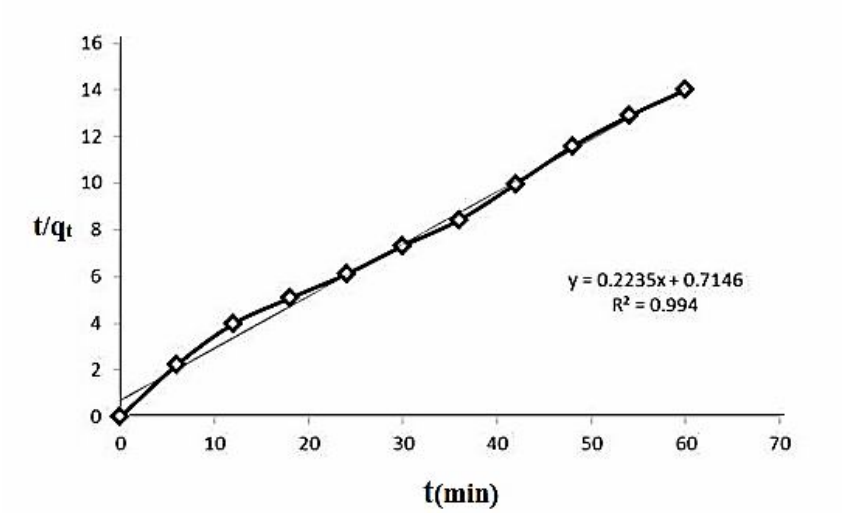

Fig. 8. The pseudo-second order kinetic model of Bisphenol- A adsorption onto HAp:Zeolite nanocomposite.

$$\Delta G = - RT\ln K_c \quad (5)$$

R refers to the universal gas constant (8.314 kJ mol^{-1} K), T is the solution temperature in Kelvin, ΔH and ΔS are the change in enthalpy and entropy of adsorption respectively and. K_c value is the equilibrium constant and calculated from Langmuir isotherm. Values of ΔH and ΔS were calculated from the slope and intercept of Vant Hoff plot ($\log K_c$ *vs*. 1/T) and represented in Table 4. The negative value of ΔH indicated the exothermic process of adsorption, evidenced by decreasing removal percentage in high temperatures. Gibbs free energy in each temperature was founded negative, which demonstrated spontaneity and feasibility of the adsorption. Finally, a negative change in entropy value showed stability, good affinity, and decrease of BPA's randomness by HAp:Zeolite nanocomposite during the adsorption process [44]. Also, Fig. 10 shows the percent of BPA adsorbed by HAp:Zeolite at three different temperatures with increasing contact time until 60 min. Results indicated that increasing contact time causes to

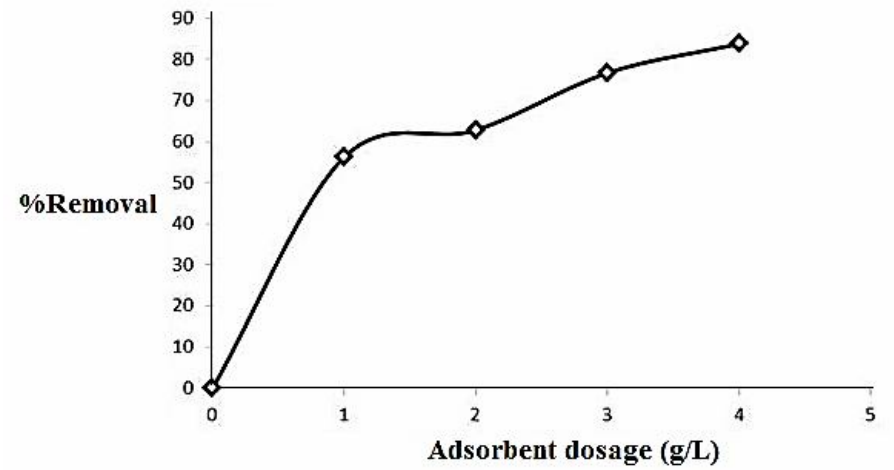

Fig. 9. Effect of adsorbent dosage on removal of BPA by HAp:Zeolite nanocomposite.

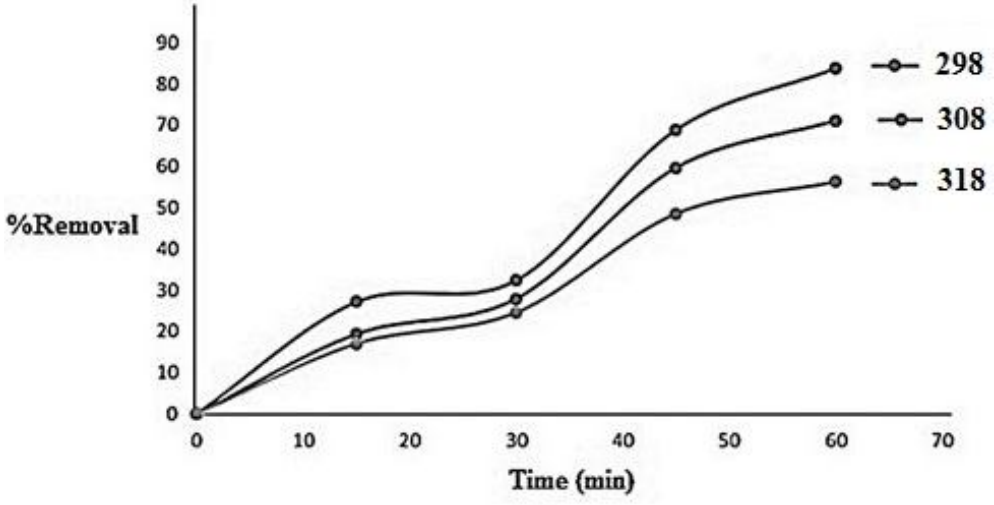

Fig. 10. Effect of temperature on removal of BPA by HAp:Zeolite nanocomposite.

Table 4. Effect of Different Types of HAp:Zeolite on Removal of BPA

Adsorbent	HPLC data (Area)	%Removal of BPA
HAp:Zeolite (1:1)	207594	57
HAp:Zeolite (2:1)	245190	49
HAp:Zeolite (4:1)	274561	42.8
HAp:Zeolite (6:1)	301347	37.05

increase percent in the removal of BPA by nanocomposite while all percent decreased by increasing temperature.

Table 4. Thermodynamic parameters for BPA removed by HAp:Zeolite nanocomposite.

Sorption isotherm. BPA uptake was quantitatively evaluated using the Langmuir, Freundlich and Dubinin-Radushkevich (DR) models at an optimum temperature of 298 K. All parameters from these models calculated, and results were shown in Table 5. Due to the correlation constant (R^2), the Freundlich model better-described the BPA sorption by HAp:Zeolite. This model can be applied to describe the reversible adsorption process occurring on the heterogeneous surface as well as multilayer sorption. The linear form of the Freundlich model is expressed by the following equation [45]:

$$\ln q_e = \ln K_f + \frac{1}{n}\ln C_e \quad (6)$$

Where q_e is the amount of BPA adsorbed per unit mass of adsorbent (mg g^{-1}), C_e is the equilibrium concentration of adsorbate (mg L^{-1}), and K_f and n are Freundlich constant. From Fig. 11, the plot of $\ln q_e$ *vs.* $\ln C_e$, a straight line with slope 1/n and intercept $\ln K_f$, is obtained. In this experiment, $1/n < 1$ and $1/n \rightarrow 0$, it is possible to assume that the adsorbent was saturated with the BPA molecules since adsorption energies decreased with surface density [46]. To estimate the nature of the adsorption process as chemical or physical, the Dubinin-Radushkevich (D-R) isotherm model was also used to analyze the equilibrium adsorption data. The linear form of the D-R isotherm model was given by the following equation [47]:

$$\ln(q_e) = \ln(q_0) - K_D \varepsilon^2 \quad (7)$$

Where q_e is the amount of adsorbate adsorbed per unit of adsorbent at equilibrium time (mg g^{-1}), q_0 is the maximum adsorption capacity (mg g^{-1}), K_D is the isotherm constant related to the adsorption energy, ε is the Polanyi potential and equal to $RT\ln(1 + 1/C_e)$, R is the universal gas constant (8.314 J mol^{-1} K^{-1}), T is the temperature (kelvin), and C_e is the equilibrium concentration of adsorbate in solution (mg L^{-1}). The q_0 and K_D values can be obtained from the slope and intercept of the plot of $\ln q_e$ *vs.* ε^2. The value of mean free energy of adsorption (E), can be determined as follow [47]:

$$E = (2K_D)^{-0.5} \quad (8)$$

The magnitude of E is useful to estimate the adsorption process. If E value is below 8 kJ mol^{-1}, the adsorption type is physical adsorption, if this value is between 8 kJ mol^{-1} and 16 kJ mol^{-1}, the adsorption type can be explained by the ion-exchange process, and if the value of E is between 16 kJ mol^{-1} and 40 kJ mol^{-1}, the adsorption type is a chemical process [47]. Table 6 shows the value of E is below 8 kJ mol^{-1} so that the adsorption of BPA on to HAp:Zeolite nanocomposite is a physical process.

Adsorption and desorption study. Regeneration and reusability of adsorbent are two essential parameters for good removal agents. In the present work, regeneration experiments for HAp:Zeolite nanocomposite were conducted using 25 mL of nitric acid (0.1 N) and sodium hydroxide (0.1 N) as stripping solvent for 1 h . The process of adsorption-desorption cycles for removal and removal efficiency is shown in Fig. 12. It can be observed that approximately 82% and 55% removal efficiency was reached three times in acidic and basic solutions. With the increase of cycling times, a slight decrease was observed, and in the fifth absorption-desorption cycle, as high as 58% and 30% efficiency was obtained in acidic and basic phrases. All the above results suggested that HAp:Zeolite nanocomposite had an excellent performance for regeneration and reusability special in acidic solution. It is evident from high desorption values, that the adsorption of BPA on to HAp:Zeolite nanocomposite is physical. This result is according to E value calculated by D-R isotherm. For this purpose, we investigated the FT-IR of adsorbent after every recovery run. There were not any drastic changes in the spectrum, and they were like fresh absorbent. However, we can see some characteristic peaks such as 501) CO, CC and CH out of plane bending), 739 (CC out of plane bending), 841 (CO stretching and CC stretching in both the rings), 1230 (CC stretching in two rings), 1340 (CCH interactions in the rings), 1570 (HCH interactions), 2926 (C-H stretching vibration of the $-CH_3$) and 3406 (O-H stretching) related to BPA that absorbed on the surface of the absorbent.

Table 5. Thermodynamic Parameters for BPA Removed by HAp:Zeolite Nanocomposite

Temperature (K)	Adsorption capacity (mg g^{-1})	ΔG (KJ mol^{-1})	ΔH (J mol^{-1})	ΔS (J mol^{-1} K^{-1})	R^2
298	11.08	-2.165	-423.85	-0.5215	0.9829
308	7.645	-2.112			
318	7.0337	-1.991			

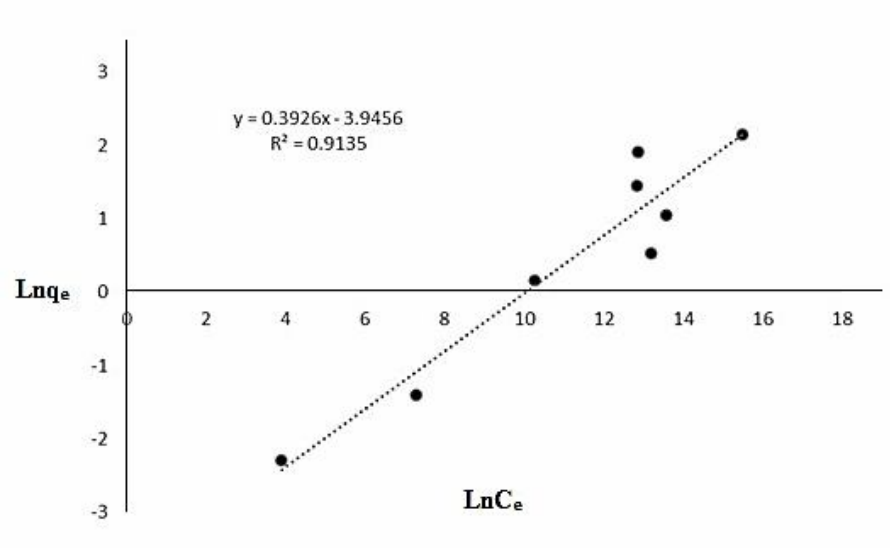

Fig. 11. Freundlich isotherm model in optimum temperature.

Comparison of HAp:Zeolite with other adsorbent. To justify the validity of the HAp:Zeolite nanocomposite as an effective adsorbent for removal of BPA, we compared our results with HAp and NaP zeolite as an adsorbent and also other works carried out elsewhere using other adsorbents for a similar purpose. We used as a basis of comparison, the maximum adsorption capacities of BPA on different adsorbents. The results are reported in Table 7, including the adsorbent used in this study. These results illustrated that higher adsorbent capacity of HAp:Zeolite nanocomposite rather than HAp and Zeolite could be due to activated site for adsorption of BPA. As compared with the adsorption capacity of other adsorbents in Table 7, HAp:Zeolite nanocomposite has a relatively good adsorption capacity.

Artificial neural network modeling. The ANN modeling technique holds several advantages over mechanistic modeling that make it particularly suitable to process modeling in the drinking water treatment industry [52]. ANN models can handle non-linear relationships and provide predictions of output parameters in real-time in response to simultaneous and independent fluctuations of the values of model input parameters.

In the present work, the prediction of total adsorption the availability of surface area and preparation of the much- by HAp:Zeolite nanocomposite was done by using three-layered feed-forward backpropagation, multi-layer perceptron (MLP) type of ANN. MLP involves an input

Table 6. Langmuir, Freundlich and D-R Sorption Isotherm Constant and Correlation Coefficient (R^2) for BPA on HAp:Zeolite Nanocomposite at 25 °C

Isotherm model	Constant parameters
Langmuir	q_m = 11.08
	K_L = 0.0016
	R^2 = 0.8228
Freundlich	K_f = 0.019
	1/n = 0.3926
	R^2 = 0.9135
D-R	K_D = 0.019
	lnq_0 = 1.4393
	E (kJ mol^{-1}) = 4.622
	R^2 = 0.6447

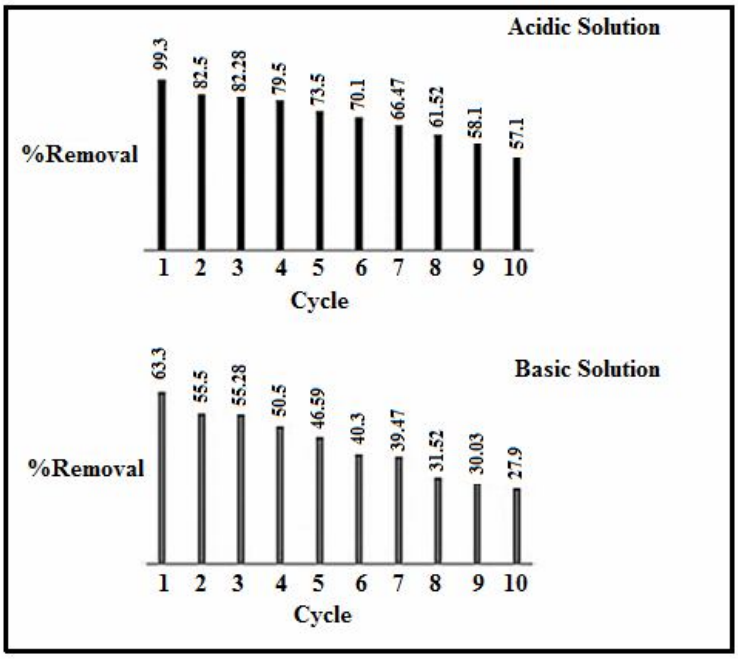

Fig. 12. Adsorption-desorption of BPA.

Table 7. Comparison of BPA Adsorption Capacity onto Several Adsorbents

Adsorption capacity of BPA by various adsorbent		
Adsorbent	Q_{max} (mg g^{-1})	Ref.
HAp	7.24	In this work
NaP:Zeolite	5.32	In this work
HAp:Zeolite	11.08	In this work
Minerals	0.33-0.86	[48]
Modified phyto-waste material	4.308-4.62	[49]
Sediment	0.15-0.3	[50]
Fe(ш)/Cr(ш) hydroxide	3.5	[51]
Andesite	<1	[48]

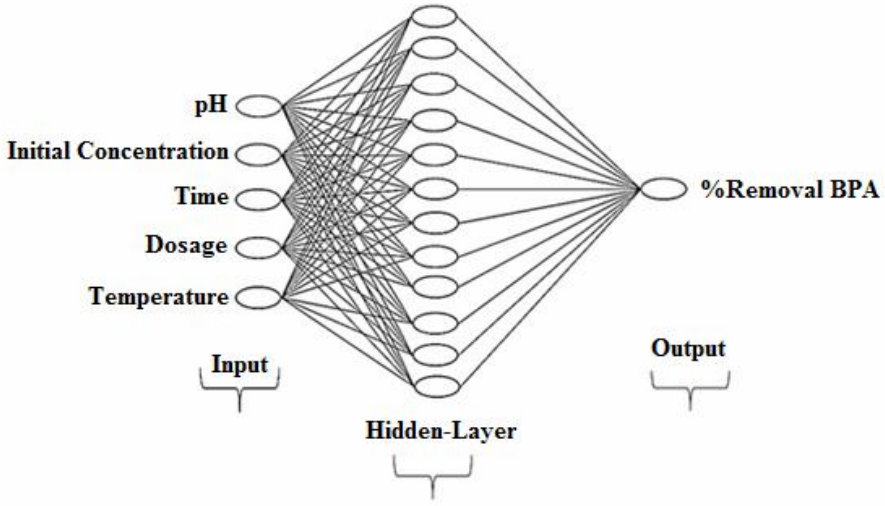

Fig. 13. The ANN optimized structure.

layer, one or more hidden layers, and an output layer. The input layer receives information from the external sources and passes this information to the network for processing. The hidden layer receives information from the input layer, does all the information processing, and output layer receives processed information from the network and sends the results out to an external receptor. The connections between the neurons are called weights. Weights can calculate the strength of the input signal. The outputs of hidden neurons are determined by passing the sum of the weighted inputs received on through a non-linear transfer or activation function. The output neurons perform the same

operations as those of hidden neurons. The hyperbolic sigmoid transfer functions have been tested in one- and two hidden layer network [22].

Seventy experimental data is divided into training and testing and validation sets. Seventy percent of data (48) is used as a training set. In contrast, fifteen percent of data (11) is used for testing for BPA, and fifteen percent of data (11) is selected for validation of the model. In order to evaluation of the validation and modeling power of the model, experimental data were selected randomly from all data.

Figure 13 shows a BP algorithm with three-layer architecture (5:12:1) with a tangent sigmoid transfer function (tansig) at the input and hidden layer and a linear transfer function (purelin) at output layer used for the modeling of BPA sorption by HAp:Zeolite nanocomposite. In this study, pH (over range 5-12), initial concentration (over the range of 5-50 ppm), contact time (over the range 30-120 min), adsorbent dosage (over range 1-4 g L^{-1}) and temperature (over range 298-318 K) was chosen as an input variable, and percent removal of BPA from aqueous solution was selected as an output variable. The network is tested with different number of neurons in range of 2-25 to the network is tested with a different number of neurons in the range of 2-25 to find the optimal number of neurons at the hidden layer by observing the mean squared error. Each topology was repeated three times. The mean square error (MSE) was applied as the error function. It measures the performance of the network according to the following equation:

$$MSE = \frac{1}{N}\sum_{i=0}^{i=N}(y_{i,pred} - y_{i,\exp})^2 \quad (9)$$

Where N is the number of data points, y_i, pred is the network prediction, y_i, exp is the experimental response, and i is an index of data. It could be seen that the network mean square error (MSE) is minimum, with the inclusion of 12 nodes in the hidden layer. Figure 14 shows the effect of the number of neurons in the hidden layer on the performance of the neural network and also used to showing the relation between the network error and the number of neurons in the hidden layer. As shown in Fig. 14, we can see the best result in 12 neurons in the hidden layer, and the network could not coverage effectively with a few neurons in the hidden layer. The weights and bias values are provided by ANN listed in Table 8. The weights are coefficients between the artificial neurons, which are analogous to synapse strengths between the axons and dendrites in real biological neurons. Therefore, each weight decides what proportion of the incoming signal will be transmitted into the neuron's body [53].

A regression analysis of the network response between ANN outputs and the corresponding targets was performed. As shown in Fig. 15, it was tried to showing correlation between predicted data and experimental data. We can see a high degree of correlation between ANN outputs (predicted data) and the corresponding targets (experimental data). Test outputs showed a very small deviation in efficiency values from the experimental data.

The performance control of ANN outputs was evaluated by determination of the correlation coefficient (R^2) which is expressed by the following equation [54]:

$$R^2 = \frac{\sum_{p=1}^{N}(t_p - t_{mean})^2 - \sum_{p=1}^{N}(t_p - o_p)^2}{\sum_{p=1}^{N}(t_p - 0_p)^2} \quad (10)$$

Where R^2 is the correlation coefficient, N is the number of the patterns, p is the index number for pattern, t_p is the target value for the p^{th} pattern, t_{mean} is the mean target value, o_p is the output of the p^{th} pattern which is produced by the ANN model.

Figure 16 illustrated the training, validation and test mean square error for the Lavenberg-Marquardt algorithm. The training was stopped after 60 epochs.

CONCLUSIONS

A detailed batch experimental study was carried out to remove BPA from aqueous solution using HAp:Zeolite nanocomposite. The optimum dose of HAP:Zeolite was found to be 4 g L^{-1} of synthetic solution. It is evident from the pH study that there was a decrease in percentage removal for an increase in pH from 7 to 12, but for further increases in pH 5 to 7, there was no efficient increase in removal. It was found from the study that the equilibrium was established after 60 min. Adsorption of BPA was found

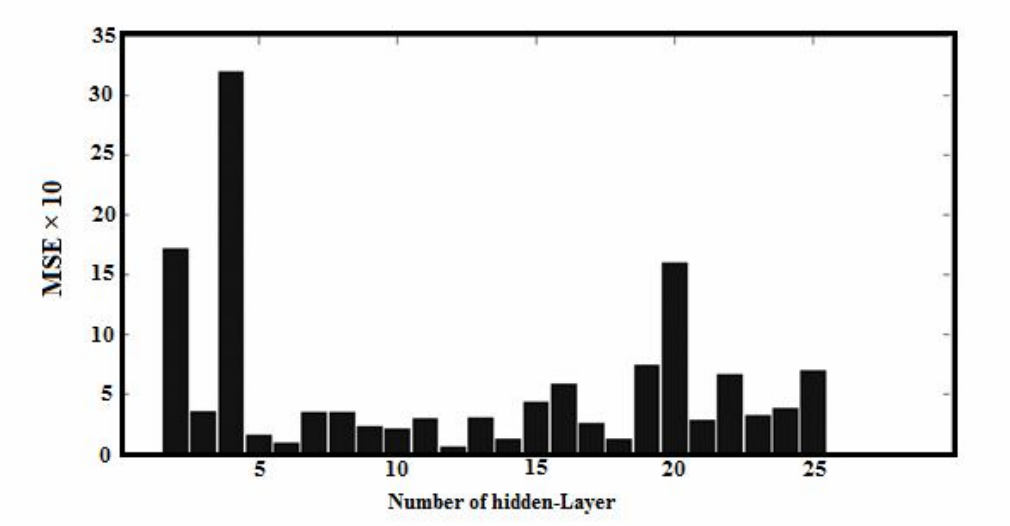

Fig. 14. Effect of the number of neurons on Hidden layer.

Table 8. Weights and Biases of the Neural Networks

W_1							W_2	
Variable								
Neuron	pH	Concentration	Time	Dosage	Temperature	Bias	Neuron	Weight
1	0.7262	1.8168	-1.3542	0.3063	3.3323	-1.5525	1	0.0128
2	-0.1259	0.7085	-1.4949	0.9170	-2.3078	-1.7034	2	-1.1668
3	0.8472	1.1868	0.8361	-0.4003	3.9132	2.3860	3	0.3760
4	0.8569	1.0447	4.6944	0.7188	-0.3577	4.0325	4	-0.1765
5	0.4040	-0.9148	0.7197	1.4985	0.6760	1.4424	5	-0.7380
6	1.1252	-1.4858	-5.2496	-0.2541	-0.3789	-1.1112	6	0.1634
7	1.3984	-0.3748	3.6164	2.6697	1.3224	0.4984	7	0.2476
8	1.5523	-1.3308	3.3849	0.4322	1.0003	-1.4374	8	0.9984
9	-0.9905	-2.093	0.9747	-0.9377	-0.0135	-2.5311	9	-0.6734
10	-2.2646	-1.0304	-0.5706	1.4465	0.4064	-1.6920	10	-1.1734
11	0.0813	-1.2182	0.9894	0.7864	2.1940	-2.2802	11	0.3564
12	1.6732	1.2135	4.7109	2.9675	3.3511	4.1152	12	1.6489
							Bias	-1.8072

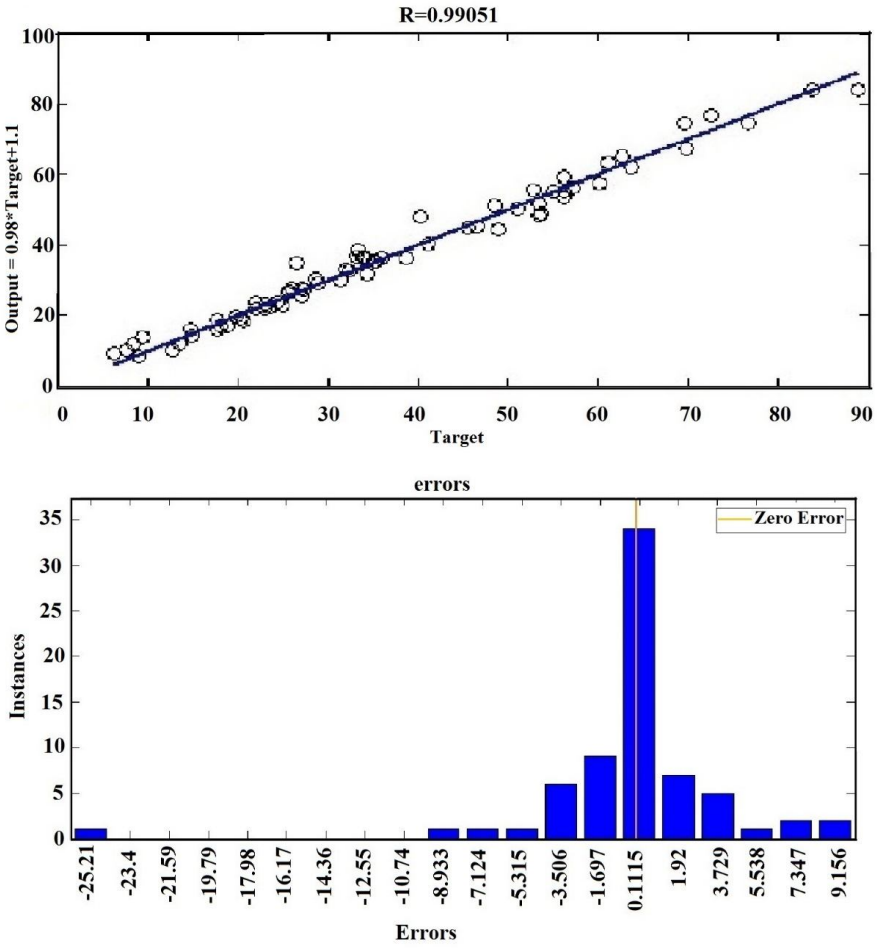

Fig. 15. Regression analysis for adsorption of BPA and Error bars.

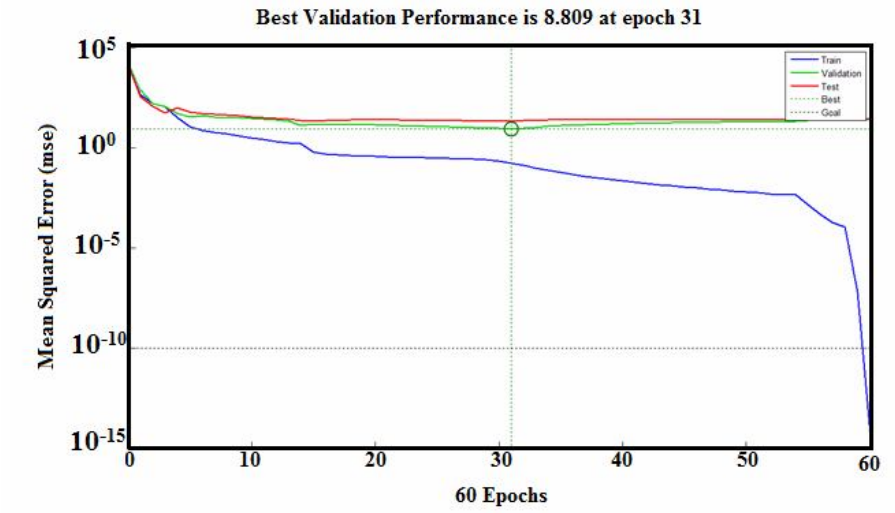

Fig. 16. ANN model training, validation and test mean squared error for Levenberg-Marquardt algorithm.

to follow second-order kinetics. The effect of temperature on the adsorption of BPA onto HAP was studied using the optimum adsorbent dose. It was observed that there was a decrease in percentage removal of BPA with an increase in temperature. The effect of initial concentration was studied and was found that the removal percentage of BPA increased from 20% to 92% by increasing initial concentration from 5 to 50 ppm. ANN model was employed for modeling of removal of BPA from aqueous solutions by HAp:Zeolite nanocomposite. A multilayer network (FFNN-MLP) with one hidden layer (5:12:1) was applied to predict the percentage removal of BPA from aqueous solution with the minimum MSE. A backpropagation algorithm was used to train the network. The model and the test data are in perfect match with an R^2 value of 0.9905. ANN successfully tracked the non-linear behavior of percentage removal of BPA versus pH, initial concentration of BPA, contact time, dosage, and temperature with low relative percentage error.

ACKNOWLEDGMENTS

Thanks to the Iranian Nanotechnology Innovation Council and the Research Council of Arak University and Center of Excellence in the Chemistry Department of Arak University and zeolite and porous materials committee of Iranian Chemical Society for supporting of this work.

REFERENCES

[1] D.P. Mohapatra, S.K. Brar, R.D. Tyagi, R.Y. Chemosphere 78 (2010) 923.

[2] H.S. Chang, K.H. Choo, B. Lee, S.J. Choi, J. Hazard. Mater. 172 (2009) 1.

[3] T. Suzuki, Y. Nakagawa, I. Takano, K. Yaguchi, K. Yasuda, Environ. Sci. Thecnol. 38 (2004) 2389.

[4] J.Q. Jiang, Q. Yin, J.L. Zhou, P. Pearce, Chemosphere 61 (2005) 544.

[5] A.V. Krishnan, P. Stathis, S.F. Permuth, L. Tokes, D. Feldman, Endocrinology 132 (1993) 2279.

[6] H.C. Alexander, D.C. Dill, L.W. Smith, P.D. Guiney, P.B. Dorn, Environ. Toxicol. Chem. 7 (1988) 19.

[7] C.A. Staples, P.B. Dorn, G.M. Klecka, S.T. O'Block, L.R. Hariis, Chemosphere 36 (1998) 2149.

[8] A. Goodson, W. Summerfield, I. Cooper, Food Addit. Contamn. 19 (2002) 796.

[9] L. Guerra, SDLP 6 (2006) 54.

[10] T. Yamamoto, A. Yasuhara, H. Shiraishi, O. Nakasugi, Chemosphere 42 (2001) 415.

[11] G. Liu, J. Ma, X. Li, Q. Qin, J. Hazard. Mater. 164 (2009) 1275.

[12] Ministry of Health, Labour and Welfare of Japan, "Exposure and Behavior Researches of Endocrine Disrupting Chemicals in Tap Water, 2000.

[13] F.R. Jiao, X.J. Sun, Z.T. Pang, Chem. Ind. 26 (2008) 21.

[14] B. Pan, D.H. Lin, H. Mashayekhi, B.S. Xing, Environ. Sci. Technol. 42 (2008) 5480.

[15] J.H. Chen, X. Huang, D.J. Lee, Process Biochem. 43 (2008) 451.

[16] Y. Wang, Sh. Jin, Q. Wang, G. Lu, J. Jiang, D. Zhu, J. Chromatogr. A 1291 (2013) 27.

[17] V.M. Mboula, V. Héquet, Y. Andrès, L.M. Pastrana-Martínez, J.M. DoñaRodríguez, A.M.T. Silva, P. Falaras, Water Res. 47 (2013) 3997.

[18] Y. Huang, D. Dong, J. Yao, L. He, J. Ho, Ch.Ch. Kong, A.J. Hill, H. Wang, J. Chem. Matter. 22 (2010) 527.

[19] J.-H. Dong, Y.-S. Lin, Ind. Eng. Chem. Res. 37 (1998) 2404.

[20] D. Zhang, H. Luo, L. Zheng, K. Wang, H. Li, Y. Wang, H. Feng, J. Hazard. Mater. 241-242 (2012) 418.

[21] M. Zendehdel, B. Shoushtari-yeganeh, G. Cruciani, JICS. 13 (2016) 1915.

[22] M. Khatamian, B. Divband, A. Jodaei, Mater. Chem. Phys. 134 (2012) 31.

[23] A. Aleboyeh, M.B. Kasiri, M.E. Olya, H. Aleboyeh, Dyes Pigm. 77 (2008) 288.

[24] G.R. Shetty, S. Chellam, J. Membrane Sci. 217 (2003) 69.

[25] J.C. Patra, G. Panda, R.N. Pal, B.N. Chatterjee, Journal of the CSI. 27 (1997) 34.

[26] M. Zendehdel, B. Shoshtari-Yeganeh, H. Khanmohamadi, G. Cruciani, Process Saf. Environ. Prot. 109 (2017) 172.

[27] A.H. Alwash, A.Z. Abdullah, N. Ismail, J. Hazard. Mater. 233-234 (2012) 184.

[28] M. Abecassis. Wolfovich, R. Jothiramalingam, M.V. Landau, M. Herskowitz, B. Viswanathan, T.K. Varadarajan, Appl. Catal. B: Environ. 59 (2005) 91.

[29] S. Hansen, U. Hakansson, L. Faelth, Acta Crystallogr. C Struct. Chem. 46 (1990) 1361.

[30] M. Sadeghi, S.L. Sharifi, H. Hatami, Int. J. Nano Dimens. 5 (2014) 91.

[31] Y. Zhan, J. Lin, J. Li, Environ. Sci. Pollut. Res. 20 (2013) 2512.

[32] Y. Wang, S. Zhang, K. Wei, N. Zhao, J. Chen, X. Mater. Lett. 60 (2006) 1484.

[33] Z. Huo, XXu, Z. Lü, J. Song, M. He, Z. Li, Q. Wang, L. Yan, Microporous Mesoporous Mater. 158 (2012) 137.

[34] S. Singh, S.B. Jonnalagadda, Bull. Chem. Soc. Ethiop 27 (2013) 57.

[35] M. Zendehdel, H. Khanmohamadi, M. Mokhtari, J. Chin. Chem. Soc. 57 (2010) 205.

[36] M.A. Bautista-Toledo, J. Ferro-García, C. Rivera-Utrilla, F.J. Moreno-Castilla, V. Fernández, Environ. Sci. Technol. 39 (2005) 6246.

[37] G. Liu, J. Ma, X. Li, Q. Qin, J. Hazard. Mater. 164 (2009) 1275.

[38] W. Janusz, E. Skwarek, The Study of Properties of Hydroxyapatite/electrolyte Interface 2 (2009). DOI: 10.2478/v10063-008-0003-x.

[39] G.R. Wiese, R.O. James, D.E. Yates, T.W. Healy, Electrochemistry of the Colloid-water Interface. In Electrochemistry of Colloid-Water Interface; Bockris J. O'M. Ed.; Int. Review Sci. Phys. Chem. Series 2; Butterworths: London, 6, 53 (1976).

[40] J. Lyklema, Fundamentals of Interface and Colloid Science. Academic Press London, 1995, pp. 3.2-3.232; b) Fundamental the Electrical Double Layers in Colloidal Systems. In Colloidal Dispersions, Goodwin J. W. Ed., Special Publication No 43; Royal Soc. Chem.: London, 47 (1981).

[41] W.T. Tsai, Ch.W. Lai, T.Y. Su, J. Hazard. Mater. B 134 (2006) 169.

[42] Q. Sui, J. Huang, Y. Liu, X. Chang, G. Ji, Sh. Deng, T. Xie, G. Yu, J. Environ. Sci. 23 (2011) 177.

[43] M. Islam, R.-K. Patel, J. Hazard. Mater. 143 (2007) 303.

[44] L. Tang, Zh. Xie, G. Zeng, H. Dong, Ch. Fan, Y. Zhou, J. Wang, Y. Deng, J. Wang, X. Wei, RSC Adv., 2016, DOI: 10.1039/C5RA27710H.

[45] Y.S. Ho, J.F. Porter, G. Mckay, Water Air Soil Pollut. 141 (2002) 1.

[46] M.M. Dávila-Jiménez, M.P. Elizalde-González, A.A. Peláez-Cid, Colloid Surface A 254 (2005) 107.

[47] H. Chen, J. Zhao, J. Wu, G. Dai, J. Hazard. Mater. 192 (2011) 246.

[48] W.T. Tsai, C.W. Lai, T.Y. Su, J. Hazard. Mater. 134 (2006) 169.

[49] Z.M. Lazim, T. Hadibarata, M.H. Puteh, Z. Yusop, Water Air Soil Pollut. 226 (2015) 1.

[50] G. Zeng, C. Zhang, G. Huang, J. Yu, Q. Wang, Chemosphere 65(2006) 1490.

[51] C. Namasivayam, S. Sumithra, Clean Technol. Environ. Policy. 9 (2007) 215.

[52] F. Despagne, D. Massart, Analyst 123 (1998) 157R.

[53] Y.M. Slokar, J. Zupan, A.M.L. Marechal, Dyes Pigm. 42 (1999) 123.

[54] H.U. Ozturk, Discharge Predictions Using ANN in Sloping Rectangular Channels with free Overfall, MSc Thesis, The Graduate School of Natural and Applied Sciences of Middle East Technical University (METU), Ankara, 2005.